On Turbulent Fluxes During Strong Winter Bora Wind Events

Nevio Babić, Željko Večenaj, Hrvoje Kozmar, Kristian Horvath, Stephan F. J. De Wekker & Branko Grisogono

Boundary-Layer Meteorology
An International Journal of Physical, Chemical and Biological Processes in the Atmospheric Boundary Layer

ISSN 0006-8314
Volume 158
Number 2

Boundary-Layer Meteorol (2016)
158:331-350
DOI 10.1007/s10546-015-0088-7

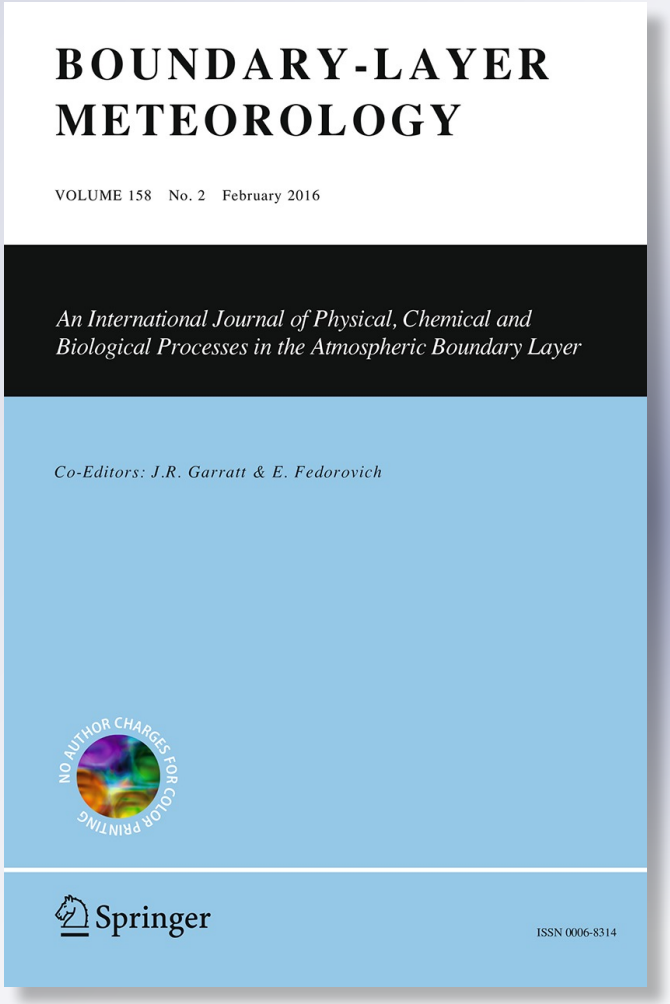

Springer

Boundary-Layer Meteorol (2016) 158:331–350
DOI 10.1007/s10546-015-0088-7

ARTICLE

On Turbulent Fluxes During Strong Winter Bora Wind Events

Nevio Babić[1] · Željko Večenaj[2] · Hrvoje Kozmar[3] · Kristian Horvath[4] · Stephan F. J. De Wekker[1] · Branko Grisogono[2]

Received: 15 December 2014 / Accepted: 3 September 2015 / Published online: 18 September 2015

Abstract Well known for its severity, the bora downslope windstorms have been extensively studied over the last several decades. This study focuses on the turbulence characteristics of bora at a topographically complex site near the eastern coast of the Adriatic Sea. For this purpose, a 3-month eddy-covariance dataset obtained at three levels (10, 22, 40 m) on a 60-m flux tower is used. After determining a suitable averaging time scale of 15 min using the fast Fourier transform and the ogive method, vertical fluxes of momentum and heat were calculated for 17 bora episodes. Up to a wind speed of 12 m s^{-1}, typical vertical profiles of momentum and heat were observed. However, for wind speeds >12 m s^{-1}, several interesting observations arose. First, the nighttime heat flux at the 10-m level was often found to be positive rather negative. Second, vertical profiles of the momentum flux were larger at the 22-m level than at 10- and 40-m levels, mostly during nearly neutral to weakly stable thermal stratification. Third, these momentum flux profiles showed a large dependence on wind direction, with virtually no vertical transport of momentum for the largest observed wind speeds. For the first time, bora coherent structures have been analyzed using the so-called variable-interval time averaging (VITA) method. The method detected coherent structures in all three wind-speed components, with structure topologies similar to those observed over forest canopies. The momentum flux increase at the 22-m level, relative to the 10- and 40-m levels, is further supported by the VITA findings.

Keywords Bora · Complex terrain · Constant-flux layer · Coherent structures · Flux divergence

✉ Nevio Babić
nb6ak@virginia.edu

1 Department of Environmental Sciences, University of Virginia, 291 McCormick Road, Charlottesville, VA 22904, USA

2 Department of Geophysics, University of Zagreb, Horvatovac 95, 10000 Zagreb, Croatia

3 Faculty of Mechanical Engineering and Naval Architecture, University of Zagreb, Ivana Lučića 5, 10000 Zagreb, Croatia

4 Meteorological and Hydrological Service, Grič 3, 10000 Zagreb, Croatia

1 Introduction

A strong, cold downslope windstorm, directed from the north-eastern quadrant over the eastern Adriatic Coast, is known as bora (Yoshino 1976; Whiteman 2000). As such, bora owes much of its reputation to its severe gustiness, often achieving wind gusts of more than 60 m s^{-1}. Bora flows nearly perpendicular to the Dinaric Alps, which approximately extend in the north-west to south-east direction, with a general increase in height and width towards the south-east (Fig. 1a).

According to extensive documentation of its climatology made during the second half of the twentieth century, the intensity and duration of bora are greatest near the major gaps in terrain (such as coastal bays) along the eastern Adriatic Coast (Jurčec 1981; Jeromel et al. 2009; Belušić et al. 2013). On the other hand, the duration of bora events shows a distinct seasonal dependence, with the longest events present during the winter season (Bajić 1989; Poje 1992; Enger and Grisogono 1998). Some of this seasonal dependence is also due to patterns in the distribution of baric formations over Europe that occur during typical bora flows. If a deep pressure low advects eastward over the Adriatic Sea, a "cyclonic" or "dark" bora usually forms, accompanied by cloudy and rainy weather (e.g. Horvath et al. 2006, 2008, 2009). In this case, a south-easterly wind, known as scirocco, may also appear on the frontside of the low. A second possible configuration includes a large and strong anticyclone over the major part of the middle and eastern Europe, in which case a "clear" bora may persist for several days, even weeks. More seldom, a third type of bora may occur (known as a "frontal" bora), in which case a strong cold front passes over the Adriatic Sea. Such events have been reported to be the shortest but often the most severe.

During the last several decades, various projects and campaigns have been conducted in an attempt to improve the understanding of bora (e.g. Grisogono and Belušić 2009). While its macroscale properties have been relatively well resolved and understood, the mesoscale characteristics of bora were initially investigated only with simple, katabatic flow models (Yoshino 1976; Jurčec 1981). However, after The Alpine Experiment (ALPEX) field campaign (Kuettner and O'Neill 1981), the importance of hydraulic theory in successfully

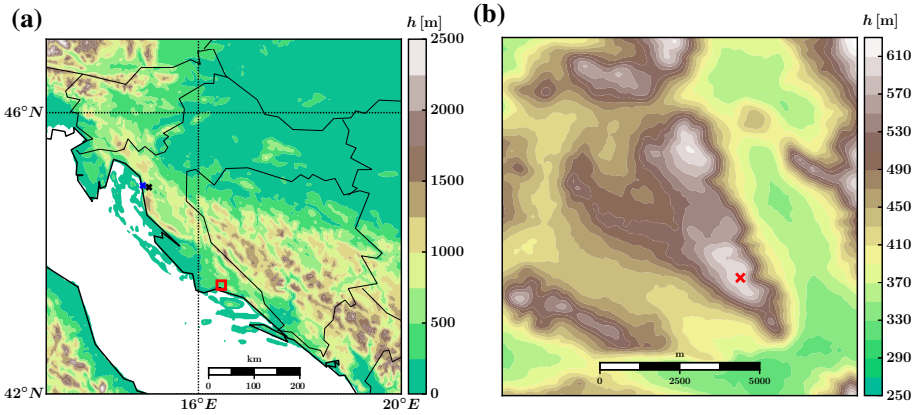

Fig. 1 **a** Map of Croatia and a part of the Adriatic Sea. The *red square* in **a** marks the **b** area around the location of Pometeno Brdo ("Swept-away Hill"). The *red cross* in **b** marks the spot of the meteorological tower. The *colour bars* denote height above mean sea level in metres. The *blue and black crosses* in **a** mark the location of Senj and Vratnik Pass, respectively

explaining bora's downslope character, at least for the north-eastern Adriatic Coast, has been repeteadly highlighted (Smith 1987; Klemp and Durran 1987; Mahrt and Gamage 1987; Bajić 1991). During the Mesoscale Alpine Programm (MAP) project (Bougeault et al. 2001), bora's mesoscale characteristics have been extensively studied (Bencetić Klaić et al. 2003; Grubišić 2004; Gohm and Mayr 2005). Following more recent advances in micrometeorological understanding during the last decade (Kaimal and Finnigan 1994; Lee et al. 2004), the main emphasis on bora research has focused on its microscale characteristics. Although the quasi-periodic nature of bora has been known for a long time (e.g. Petkovšek 1976, 1982, 1987), the nature of bora's gustiness and its pulsations have been recently addressed in more detail. Using single-point ground-based measurements in Senj, a location historically most acknowledged for bora, and Vratnik Pass at the north-eastern Adriatic Coast (Fig. 1a), Belušić et al. (2004) and Belušić and Bencetić Klaić (2006) found that the pulsations in the bora occur quasi-periodically, with periods between 3 and 11 min. This was further confirmed in a numerical modelling study by Belušić et al. (2007), who attributed the generation of gust pulsations to Kelvin-Helmholtz shear instabilities, or their absence to the formation of mountain-wave induced rotors in the lee of the Velebit mountain range. Motivated by severe turbulence developed in the wave breaking region and in the lee of the northern Dinaric Alps, Večenaj et al. (2010) addressed the issue of estimating turbulence dissipation rates during typical bora events. Using high frequency aircraft and dropsonde data obtained during the MAP field campaign, Večenaj et al. (2012) investigated along-coast bora properties and their sensitivity to different atmospheric boundary layer (ABL) parametrization schemes. With the interest of investigating wind-farming potential (Horvath et al. 2011) at the central eastern Adriatic Coast, Lepri et al. (2014) assessed features of bora wind-speed profiles during a relatively strong summer bora event. They found, by comparing power-law and logarithmic-law vertical profile approximations, that the wind-velocity profiles during intensive bora flows are substantially different compared to those during weak bora flows.

Analysis of coherent structures aids the understanding of the source, nature and variability of ABL flows. However, the nature of these structures during moderate to strong bora flows is yet to be determined. Coherent structures are generally defined as organized three-dimensional regions in turbulent flow, in which some property (e.g. temperature, wind speed, density, vorticity) is correlated with itself or another property at a time scale that is significantly larger than the smallest scale of the flow (Robinson 1991). Due to their extremely intermittent nature, coherent structures are observed in a variety of shapes and forms. Related to motions such as hairpins, vortices or plumes, coherent structures are usually traced through a sudden, temporally very localized change of a variable. In most experimental ABL studies, these changes involve ramp-like patterns with highly variable intensities and durations (Krusche and Oliveira 2004; Thomas and Foken 2007; Segalini and Alfredsson 2012). In an attempt to bridge the gap between idealized geometrical and observed shapes, Belušić and Mahrt (2012) have shown that coherent motions in the atmosphere can be approximated using four basic shapes: sine, ramp-cliff, cliff-ramp and step shape functions. With the development of high-frequency instrumentation, coherent structures have been intensively documented in recent years. Using simple and robust conditional averaging techniques, such as quadrant analysis, variable-interval time averaging (VITA) or principal component analysis (PCA), the importance of turbulent transport below and above forest canopies has been very well documented. More so, the development of the more advanced wavelet covariance technique has enabled precise detection of coherent structures (Feigenwinter and Vogt 2005; Barthlott et al. 2007; Thomas and Foken 2007; Zeri and Sá 2011; Horiguchi et al. 2012; Segalini and Alfredsson 2012). Studies investigating coherent structure evolution over complex terrain

are not as abundant (Cava et al. 2005; Helgason and Pomeroy 2012). To our knowledge, the above techniques have not been applied yet to high-frequency bora measurements.

For investigating ABL flow structure over complex terrain, the majority of experimental campaigns are designed so that the influence of upwind terrain heterogeneities is minimized. For instance, the Bolund experiment (Bechmann et al. 2011; Berg et al. 2011; Diebold et al. 2013) took place over an eliptically shaped peninsula, surrounded by sea from nearly all sides, resulting in an extended upwind homogeneous fetch. Another example is the Askervein Hill, an eliptical hill surrounded by low and uniform vegetation, again resulting in fetches that are highly homogeneous and ideal for numerical modelling (Undheim et al. 2006; Lopes et al. 2007; Moreira et al. 2012). Most recently, Grant et al. (2015) investigated airflow observations at Leac Gharbh, a forested ridge located off the Scottish mainland. This site was also characterized by a relatively homogeneous upwind fetch. Despite the above studies, there is still a lack of observational, theoretical and numerical studies in the literature, detailing flow over complex terrain. This holds especially for the Dinaric Alps, where homogeneous upwind conditions are rarely present.

The present study analyzes wintertime high-frequency bora measurements, obtained on a 3-level tower at a central location of the eastern Adriatic Coast, where bora has not been studied well. We investigate profiles of the kinematic vertical fluxes of momentum and heat, which are the basic components of momentum and heat budget equations, respectively. To properly define these fluxes, we determine a suitable averaging time scale via spectral analysis. We also assess the degree of the vertical flux divergence, which, if substantial, might question the validity of the constant-flux layer assumption in Monin-Obukhov similarity theory (MOST, Monin and Obukhov 1954). MOST states that in the surface layer (also known as the inertial sublayer), fluxes generally vary within 10 % of their surface values. This, in turn, may have important implications for applying MOST to simulating bora and other transient flows developed over topographically complex terrain. Due to a lack of studies that closely address the vertical structure of fluxes in the surface layer, it is unknown how valid this assumption is for windstorm events in general. In numerical weather prediction models, the constant-flux layer assumption is most often invoked as a matter of convenience, partly because the lowest vertical grid points may not even encompass the surface layer. This issue is even more challenging with the increasing use of mesoscale models at kilometre or finer grid spacings over complex terrain (Horvath et al. 2012).

2 Data and Methods

The site of Pometeno Brdo ("Swept-away Hill") is located on the windward side of Split, Croatia, the largest city on the eastern Adriatic Coast. The hill itself is oriented in the north-west to south-east direction of the Dinaric Alps (Fig. 1a). Along this axis towards the south-east, the hill decreases in width and, on average, increases in height (Fig. 1b). Additionally, the windward slopes are steeper and characterized by more pronounced terrain heterogeneities compared to the leeward slopes, with an occassional crevice or hollow several tens of m deep in the vicinity of the tower. The surface of the hill is mostly covered with shrubs and coppices, rarely over 2 m tall. To the south of the measurement tower, a single wind turbine was located approximately 100 m away. While operational, this turbine may have influenced the measurements at the tower for wind directions in the range 130°-190° (estimated by taking into account the typical angle between the wind direction and wake border of the turbine, yaw control, length of blades and the azimuth between the measurement tower and the turbine

itself). For the north-east sector, from which direction the bora usually occurs, it is unlikely that the turbine had any influence on bora measurements. To the east and south, the hill is surrounded by regional roads several km away, thus making this location easily accessible for construction and maintenance of wind-energy structures. Moreover, the orientation relative to the well-established bora flow makes this location particularly favourable for wind farming.

The data used herein were collected on a 60-m tall tower from 1 January 2011, 0000 UTC to 31 March 2011, 2359 UTC. The tower was located on top of Pometeno Brdo (approximately 620 m above mean sea level (a.m.s.l.), Fig. 1b). Three-dimensional wind velocity and sonic temperature were sampled with WindMaster Pro (Gill Instruments) ultrasonic anemometers at 10, 22 and 40 m above ground level (a.g.l.). The sampling frequency of the anemometers was set to 5 Hz, the highest rate with which bora has been sampled to date. The data were collected using a CR1000 datalogger (Campbell Scientific, Inc.). All three anemometers were mounted at the end of 2-m long aluminum booms to reduce distortion influences from the tower. In addition, the booms pointed toward the north-east, in order to fully capture the entire span of bora directions. Quality check of the dataset included despiking and removal of all questionable and erroneous outliers (Vickers and Mahrt 1997). Additionally, since our aim was to obtain a dataset suitable for spectral analysis, all missing datapoints were linearly interpolated. Such values were statistically insignificant and very low (less than 5 % of the total number of data samples). Time series were further block-averaged into 30-min intervals, and an appropriate coordinate rotation into streamwise u and lateral v wind-speed components was made. The rotation was performed by rotating the Cartesian coordinate system into the linearly interpolated mean wind direction at the 25-m level (mid-level between 10 and 40 m). Since the issue of properly rotating the coordinate system needs to be addressed over complex terrain, we have also performed a double rotation, as well as a planar-fit rotation (Wilczak et al. 2001), to check for possible discrepancies. No significant differences in the resulting momentum and heat fluxes were observed (not shown).

In total, 17 bora episodes were extrapolated from this 3-month observational period, based on two criteria: 10-min averages of wind direction on all three levels had to be from the north-eastern quadrant (namely, 25° to 85°), and such behaviour had to persist for at least 10 h. All 17 episodes were evenly distributed over the observational period. The cumulative duration of all episodes was 539 h, with the shortest episode lasting 10 h and the longest episode lasting 123 h. Analysis of prevailing synoptic conditions indicated that both cyclonic and anticyclonic bora were represented equally. At the 10-m level, mean wind speeds of all bora episodes ranged from 4.3 to 14.6 m s^{-1}, while the strongest observed gusts did not exceed 34 m s^{-1}.

3 Results

3.1 Averaging Time Scale

To separate turbulent perturbations (needed for the calculation of EC quantities such as variances and covariances) from the mesoscale atmospheric motions, a suitable time-averaging interval (time scale) is required. This averaging interval is most commonly represented as a local minimum in the power spectral densities of various turbulence quantities, such as wind speed, potential temperature and other scalar quantities. The essence of Reynolds-decomposition, which is normally used to separate an instantaneous signal into its mean and fluctuating components, lies in the implicit assumption that such a minimum exists (Reynolds 1894; Van der Hoven 1957; Stull 1988). Additional motivation for decomposing the data in

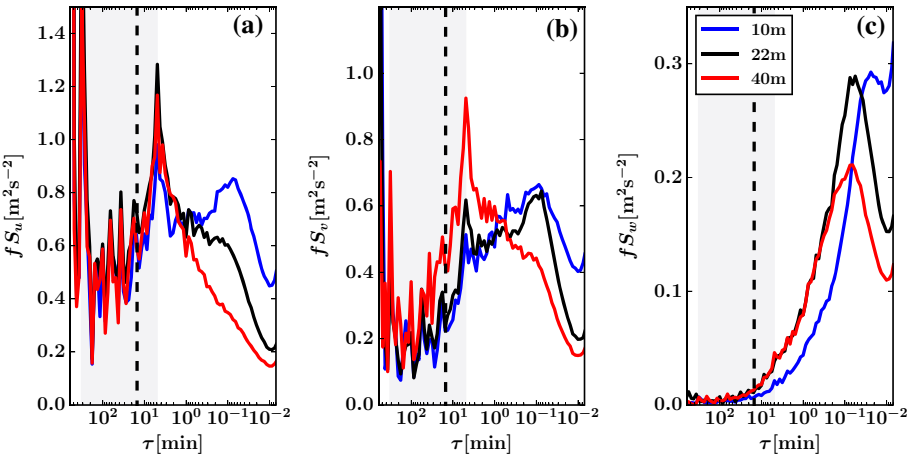

Fig. 2 Log-linear representation of the frequency-weighted power spectral densities of the, **a** longitudinal (u), **b** lateral (v) and **c** vertical (w) wind-speed components for all three heights, for the longest bora episode (123 h). The *grey shaded area* (5–316 min) represents the hypothetical mesoscale energy minimum, while the *vertical dashed line* marks the 15-min period

such a way might be to address non-stationarity in a time series, since all observations are inherently non-stationary to some extent (Mahrt 2007; Večenaj and De Wekker 2014).

Due to a large number of bora episodes available for further analysis, we focus only on the longest, i.e. 123-h long episode. The episode lasted from 21 February, 0815 (LST = UTC+1) until 26 February, 1115 (LST) 2011. This was a typical anticyclonic ("clear") bora episode, where a large, relatively stationary anticyclone (Siberian High) was located over much of Europe. Simultaneously, a deep pressure low formed over the Tyrrhenian Sea and gradually moved eastward toward the Aegean Sea during this bora episode. This ensured longevity and continuity of gusty flow, which was most severe during 24 and 25 February.

Using Fourier spectral analysis, namely the fast Fourier transform (FFT), weighted power spectral densities of all three wind-speed components were calculated for this episode, using a single window equal to 2^{21} datapoints. After smoothing the spectral amplitudes by block averaging (Kaimal and Finnigan 1994), a relatively broad minimum was observed in the weighted spectra of u and v wind-speed components on all three levels (Fig. 2a, b), between frequencies corresponding to periods of 5 and 316 min. The energy peak appearing at the 5-min period in the spectra of both horizontal wind-speed components is indicative of gust pulsations (Belušić et al. 2004, 2007). It was not possible to observe a clear minimum in the spectra of the vertical w wind-speed component (Fig. 2c). As expected, the u component contains most of the wind energy, according to the orders of magnitude of the y-axes, indicating strong anisotropy of the bora flow at this site. We hypothesize that the averaging time scale might correspond to approximately 15 min, as this is the last significant minimum before the 5-min peak is reached. In this way, we can make sure not to underestimate turbulent fluxes by choosing a too small value for the time scale nor to overestimate the fluxes by choosing a too large time scale. However, since this approach is still somewhat subjective and relies largely on visualization of the spectra, further confirmation of the proposed choice of the averaging time scale is required.

To more accurately pinpoint the most suitable averaging time scale for winter-time bora at Pometeno Brdo, cumulative flux integrals (ogives) were calculated from cospectra of

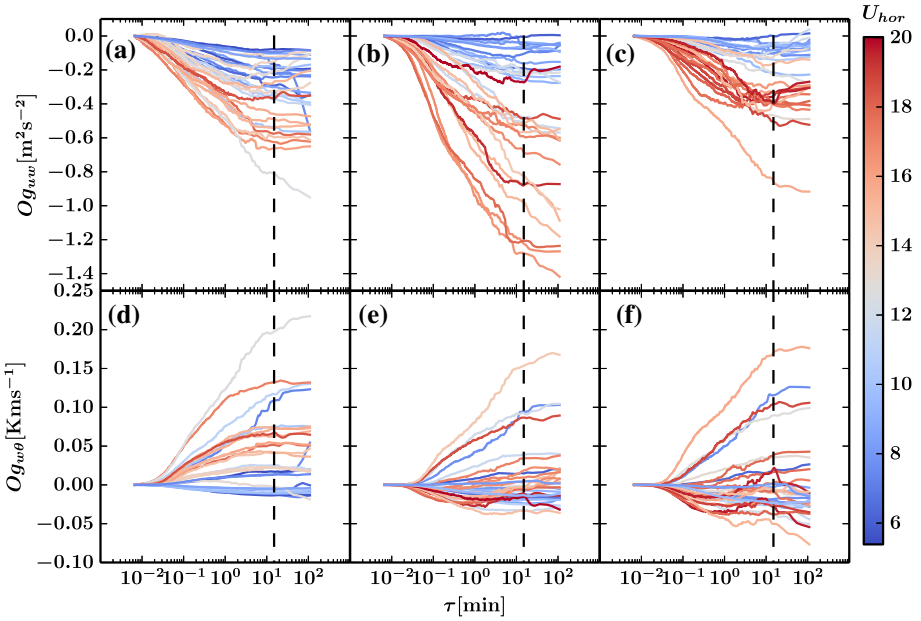

Fig. 3 Log-linear representation of ogives of kinematic vertical fluxes of momentum at, **a** 10, **b** 22 and **c** 40 m heights, and of ogives of kinematic vertical fluxes of heat at, **d** 10, **e** 22 and **f** 40 m heights, for the longest bora episode (123 h). All ogives are colour-coded based on the mean horizontal wind speed (right-most colour bar) for particular ogives' 4-h segment. The *vertical dashed line* marks the 15-min period

kinematic vertical fluxes of momentum and heat (Oncley et al. 1996; Moncrieff et al. 2004; Metzger and Holmes 2008; Večenaj et al. 2011; Babić et al. 2012; Helgason and Pomeroy 2012; Večenaj et al. 2012),

$$Og_{xy}(f_0) = \int_{\infty}^{f_0} Co_{xy}(f)\,\mathrm{d}f. \tag{1}$$

In Eq. 1, Co_{xy} denotes Fourier cospectra of a function of any two variables, x and y, while f_0 represents the frequency of the associated averaging time scale. The integration is performed from infinite frequencies (in practice, the Nyquist frequency = 2.5 Hz for this study) towards lower frequencies (longer periods). When the cospectrum does not substantially contribute to the ogive at frequencies lower than f_0, the inverse of this frequency can be interpreted as the averaging time scale. After each bora episode was partitioned into 4-h segments following Foken et al. (2006), cospectra of momentum and kinematic heat were calculated for each segment using windows with 2^{16} datapoints. The resulting ogives for this longest captured bora episode are plotted in Fig. 3. An additional justification for choosing this particular 5-day event was to ensure that the conclusions derived from the ogive analysis are statistically significant, since this event has the largest number of ogives (30) encompassing both weak and strong bora sub-events.

The cospectrum Co_{uw} does not seem to contribute significantly to the ogive at periods beyond approximately 15 min (Fig. 3a–c), thus strenghtening our hypothesis that this period can be representative of the 5 to 316 min minimum in the weighted spectra (Fig. 2a, b). On average, regardless of each ogives' mean wind speed, they all achieve a certain level of convergence beyond 15 min. This is further confirmed by ogives of cospectra of the heat flux

$Co_{w\theta}$ on all three levels (Fig. 3d–f), which show a more consistent leveling-off for periods longer than 15 min, regardless of the bora wind-speed. Hence, hereafter we use the averaging time scale of 15 min to define turbulent perturbations of the wind-speed components and sonic temperature. Although a more complete and objective estimate of the averaging time scale might still be possible, through the employment of higher order spectral methods, for example the multiresolution flux decomposition (Vickers and Mahrt 2006; Metzger and Holmes 2008; Večenaj et al. 2012), the Hilbert-Huang transform (Huang et al. 1998; Lundquist 2003) or the wavelet covariance technique (Torrence and Compo 1998; Grinsted et al. 2004), we believe that for present purposes the averaging time scale is obtained adequately.

Ogives of the momentum flux tend to have lower values in the low-frequency end of the spectrum for lower than for higher wind speeds, indicating that turbulent mixing is weaker when bora is weak to moderate (5–10 m s^{-1}). Surprisingly, when bora becomes more intense (exceeding approximately 12 m s^{-1}), ogives of the momentum flux in the low-frequency range at the 22-m level (Fig. 3b) have much higher values, compared to those at the 10- and 40-m levels. Since the value of the ogive at the low-frequency end of the spectrum (100 min) is proportional to the segment mean flux, this observation would imply strongest downward transport of momentum at the 22-m level, relative to the other two measurement levels. Ogive analysis of other bora episodes, especially the stronger and longer ones, confirms the behaviour observed above (not shown).

We next discuss the temporal evolution of the mean wind speed, vertical fluxes, and wind direction for this 5-day event (Fig. 4). While the wind was still relatively weak (21 and 22 February, Fig. 4a), both momentum fluxes $\overline{u'w'}$ and $\overline{v'w'}$ were approximately constant across all three levels, showing a slight downward transport of momentum (Fig. 4b, c). Early on 23 February, the wind speed, as well as the gustiness, steadily increased, reaching maximum values on 24 and 25 February. Meanwhile, during passage of the pressure low over southern Greece during 24 and 25 February, the upper-level geostrophic flow was nearly perpendicular to the Dinaric Alps, strenghtening the bora flow during this period. Coincidentally, the fluxes increased in magnitude, indicating stronger turbulent mixing (Fig. 4b). However, both momentum fluxes $\overline{u'w'}$ and $\overline{v'w'}$ show a clear increase at the 22-m level throughout this entire 2-day period, reaching values of -1.7 and -1.2 m^2 s^{-2}, respectively. As the wind speed decreased suddenly at the end of the episode, the momentum fluxes follow that trend, decreasing in magnitude and, more importantly, again becoming relatively constant with height. This behaviour of the momentum fluxes at the 22-m level is a clear confirmation of the conclusions based on ogives, indicating stronger momentum flux at the 22-m level in comparison with the other two measurement levels. As for the vertical heat flux $\overline{w'\theta'}$ (Fig. 4d), an obvious diurnal trend is visible, indicating strong upward transport of heat during the day. A weaker downward transport of heat can be observed during the night than during the day. Similarly to the momentum flux, during periods with strongest wind speeds (24 and 25 February), the vertical heat flux $\overline{w'\theta'}$ at the 10 m level remains positive, even during nighttime. This observation is also reflected in the ogives of the heat flux at the 10-m level (Fig. 3d), where all high speed ogives remain positive over the entire frequency range. This is not the case at the 22- and 40-m levels, where a nighttime downward transport of heat does occur during the strong bora flow. Sensitivity of the fluxes on the wind direction does seem a possibility (Fig. 4e). It is evident that during 24 and 25 February the flow is more uniform with height than during periods of weaker bora winds. Since the flow could be influenced by the subtle heterogeneities of the underlying terrain upwind of the tower, we assess the height dependence of the momentum fluxes in more detail in Sect. 3.4.

Based on the above observations, a constant-flux layer might be very shallow, if not completely absent, at Pometeno Brdo for bora wind speeds $\gtrsim$ 12 m s^{-1}. The remainder of

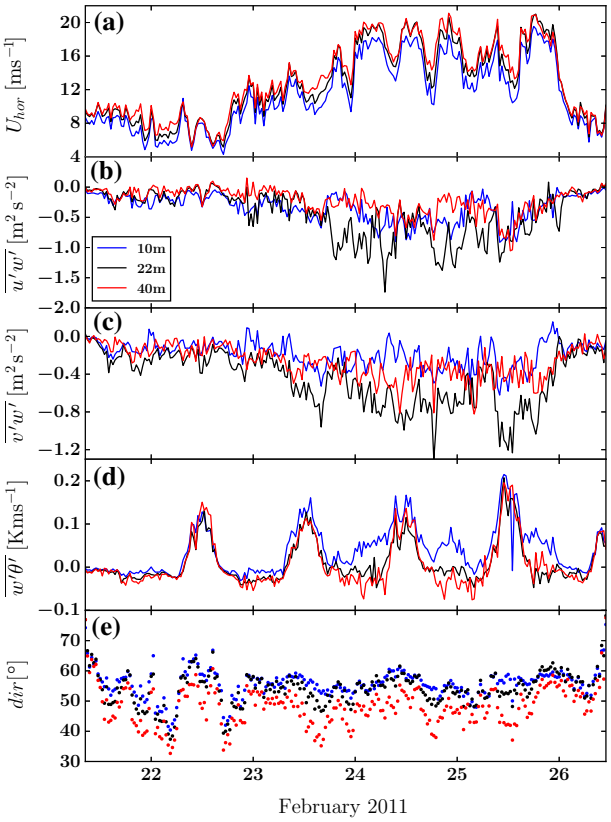

Fig. 4 Time series of **a** mean horizontal wind speed, **b** vertical momentum flux $\overline{u'w'}$, **c** vertical momentum flux $\overline{v'w'}$, **d** vertical heat flux $\overline{w'\theta'}$ and **e** wind direction on all three heights, for the longest bora episode (123 h)

the study focuses on explaining the nature and possible origin of this flux divergence using spectral, stability, directional footprint and coherent structure dedicated analyses.

3.2 Spectral Analysis of Vertical Fluxes

Since frequency-weighted spectra, when plotted on a log-linear scale, preserve areas under the spectral curves (e.g. Kaimal and Finnigan 1994), we can interpret those areas as variances of each of the wind-speed components. In the following analysis, we only compare spectral areas of the vertical wind-speed component $fS_w(f)$, since these show the least between-episode variability in terms of minor spectral peaks of questionable origin and scale. When plotted as a function of the episode mean wind speed at the 22-m level (Fig. 5), differences in the area under the weighted spectra of the vertical wind component show that the area under the 22-m curve becomes greater than those at the other two levels, when mean wind speeds $\gtrsim$ 12 m s^{-1}. Plotting gustiness of the vertical wind component for strong bora episodes (not shown) revealed that the gustiness attained its highest values exactly at the 22-m level. Stronger gustiness may imply, on average, larger turbulent perturbations, and thus might explain the reason for the momentum flux behaviour at the 22-m level shown earlier, since the resulting covariance would increase in magnitude.

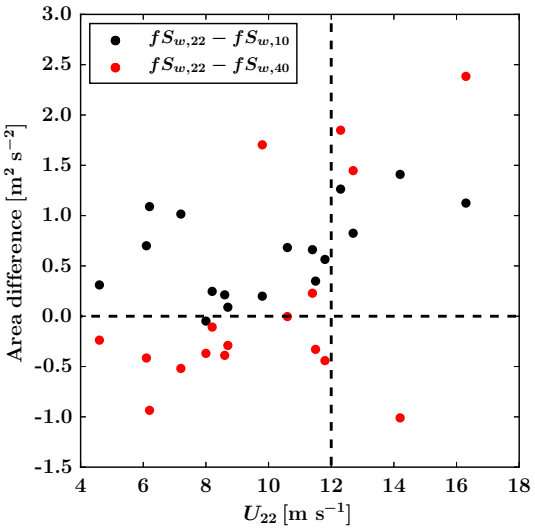

Fig. 5 Scatterplot of the difference in the area under the frequency-weighted power spectral densities of the vertical wind-speed component as a function of the mean wind speed at the 22-m level, for all 17 episodes. The *horizontal dashed line* marks the border of equal spectral areas, while the *vertical dashed line* corresponds to a wind speed of 12 m s^{-1}

3.3 Stability Analysis of Vertical Fluxes

Using the eddy-covariance technique enables us to look more closely at the nature of the static stability of the bora (Lepri et al. 2014). For this purpose, the non-dimensional stability parameter ζ is calculated for all 17 bora episodes on all levels (Stull 1988),

$$\zeta = \frac{z}{L}, \tag{2a}$$

$$L = -\frac{u_*^3 \overline{\theta_v}}{\kappa g \overline{w'\theta_v'}}. \tag{2b}$$

where z represents the measurement level, L is the Obukhov length (Monin and Obukhov 1954), $\kappa = 0.4$ is the von Karman constant (e.g. Högström 1996), $g = 9.81\,\mathrm{m\,s^{-2}}$ is the acceleration due to gravity, $\overline{w'\theta'}$ is the local vertical heat flux, u_* is the local friction velocity and θ_v is the virtual potential temperature. Since no direct measurement of relative humidity was made, we make the assumption that the sonic temperature is a relatively good approximation to the virtual potential temperature (Fortuniak et al. 2013; Nadeau et al. 2013; Večenaj and De Wekker 2014).

Plotting all the variables in Fig. 4, now as functions of ζ, is shown in Fig. 6, where each bin is represented by its median value in order to achieve smoother curves and to mitigate the influence of outliers. As in Grachev et al. (2005), we advise some caution when interpreting this figure, since partial correlation between the fluxes and ζ may be due to self-correlation. Since the majority of the 17 episodes occured during nighttime conditions, we have a higher concentration of datapoints on the statically stable side. As expected, wind speeds increase as statically near-neutral conditions are achieved from both unstable and stable sides (Fig. 6a). Figure 6b, c clearly show that the unusual momentum flux pattern at the 22-m level occurs mainly during near-neutral conditions, especially on the statically stable side ($0 < \zeta < 0.02$), corresponding to wind speeds $\gtrsim 12\,\mathrm{m\,s^{-1}}$ at the 22-m level. This confirms our remarks based on Figs. 3 and 5, i.e. that this behaviour persists only during strong bora flows. During statically unstable conditions, the momentum flux $\overline{v'w'}$ resembles the shape of its stable counterpart; however, the same does not hold for $\overline{u'w'}$. The values of

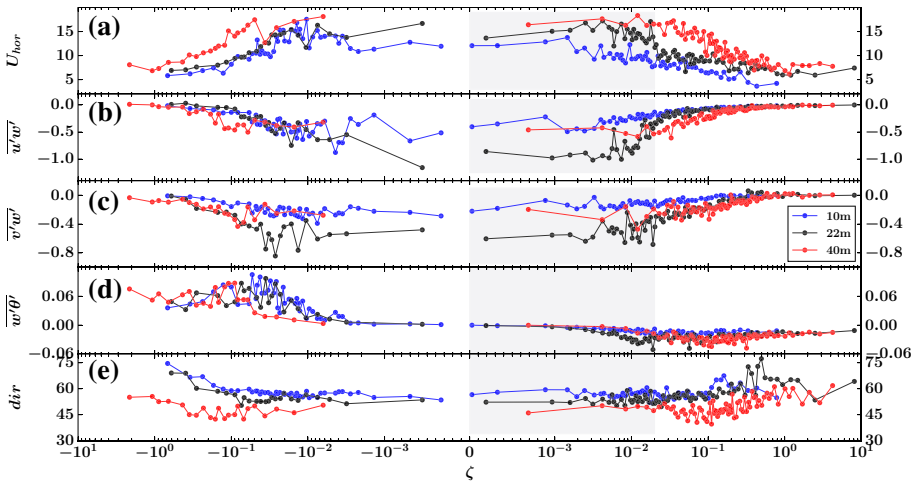

Fig. 6 Bin average composites (medians shown) of **a** mean horizontal wind speed U_{hor}, **b** vertical momentum flux $\overline{u'w'}$, **c** vertical momentum flux $\overline{v'w'}$, **d** vertical heat flux $\overline{w'\theta'}$ and **e** wind direction on all three heights and for all 17 bora episodes. *Grey shaded area* ($0 < \zeta < 0.02$) marks the stability region with the observed momentum flux at the 22-m level being greater than that at the adjacent levels. Units as in Fig. 4

the heat flux $\overline{w'\theta'}$ and therefore the transport of heat, are generally larger during statically unstable stratification than during stable stratification (Fig. 6d).

By inspecting the normalized absolute differences of all three vertical fluxes between two adjacent levels (Grachev et al. 2005), and thus defining two mid-levels (16 and 31 m), we can quantify the flux-divergence coefficient according to,

$$K = \left| \frac{\{\overline{u'w'},\ \overline{v'w'},\ \overline{w'\theta'}\}_{\text{upper}} - \{\overline{u'w'},\ \overline{v'w'},\ \overline{w'\theta'}\}_{\text{lower}}}{\{\overline{u'w'},\ \overline{v'w'},\ \overline{w'\theta'}\}_{\text{lower}}} \right| \leq 10\,\%. \tag{3}$$

When plotted as a function of the stability parameter ζ (Fig. 7), both momentum fluxes $\overline{u'w'}$ and $\overline{v'w'}$ fail to support any presence of a constant-flux layer throughout the entire unstable and stable thermal stratification, especially at the lower, 16-m mid-level (Fig. 7a, b). Characterized also by high variability of the flux-divergence coefficient K (15–300 %), it is obvious that surface-layer similarity (MOST) is not valid at this mid-level, since the friction velocities above (22 m) and below (10 m) the 16-m mid-level are not coupled. The flux divergence is somewhat lower and shows less variability at the upper mid-level (31 m), but the K values are still too large (30–60 %). Despite the fact that there are no additional levels above 40 m, we hypothesize that the flux divergence may continue to decrease with height. In the case of the heat flux $\overline{w'\theta'}$ (Fig. 7c), the fluxes seem to be less divergent with height, especially in the free convection limit ($\zeta < -0.05$) and during moderately stable stratification ($\zeta > 0.1$) at the 31-m mid-level. Caution is advised when interpreting large values of the heat flux divergence K very close to statically near-neutral conditions ($|\zeta| < 0.02$), since these values may be an artefact of normalizing the difference in Eq. 3 with very small values of the heat flux (Fig. 4d).

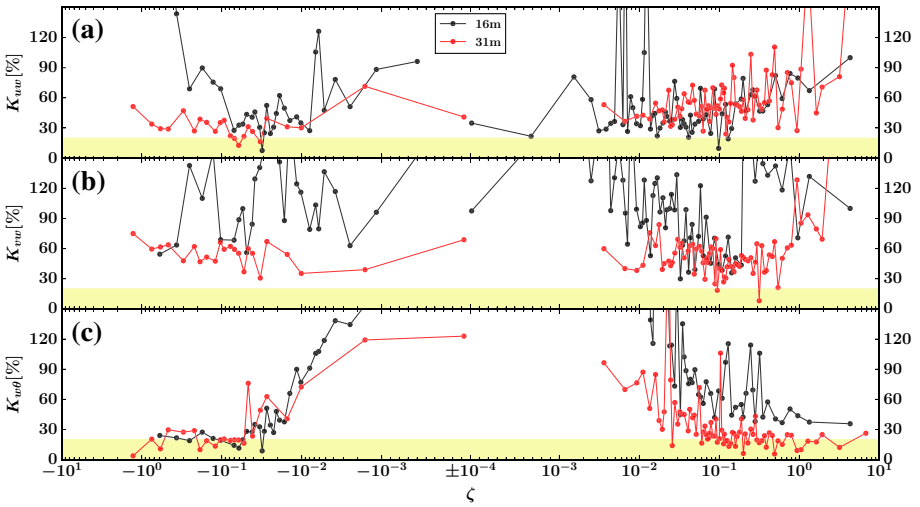

Fig. 7 Bin average composites (medians shown) of the flux-divergence coefficient given in (3), for **a** vertical momentum flux $\overline{u'w'}$, **b** vertical momentum flux $\overline{v'w'}$ and **c** vertical heat flux $\overline{w'\theta'}$ on all three heights and for all 17 bora episodes. *Colour* representing both mid-levels is given in the legend. *Yellow shaded area* at the *bottom* of all subplots represents the constant-flux layer (less than 10 % flux variability with height)

3.4 Sensitivity of Vertical Momentum Fluxes on Wind Direction

A potential dependence of the wind-directional shear as a function of wind speed has been postulated in Sect. 3.1. (Fig. 4e). To further explore this dependency, we plot 30-min averages of the $\overline{u'w'}$ momentum flux as a function of the wind speed, for all levels and for all registered bora episodes (Fig. 8). A generally northward, counter-clockwise turning of the wind with height is evident. Again, the momentum fluxes at the 22-m level appear higher than those at the adjacent levels, but their distribution is highly dependent on the wind speed. For example, the maxima in the momentum flux seem to behave as a nearly linear function of the wind speed, since these are associated with 15 m s^{-1} (10 m), 17 m s^{-1} (22 m) and 18 m s^{-1} (40 m) wind speeds at these three heights, respectively. Furthermore, the downward momentum transport decreases with wind speeds beyond the above values, possibly due to respective terrain-induced separation of the flow, recirculation, and reattachment phenomena. Surprisingly, at the 10- and 22-m levels, wind speeds of 14 m s^{-1} and 17 m s^{-1}, respectively, mark the onset of a momentum flux sign reversal, with a clear distinction between two different regimes of the momentum flux that continue to persist at higher wind speeds. The first regime, associated with wind directions of 52° to 60°, seems to characterize weaker downward (in some cases even an upward) transport of momentum compared to the second regime, which is associated with wind directions of 45° to 52°. As wind speeds increase, the second regime ceases to exist at both levels, and only the first regime remains. Thus, the strongest bora flow at Pometeno Brdo is characterized by almost zero vertical transport of momentum. The above finding can also be extended to the 40-m level, where the momentum flux reverses sign at speeds equal to approximately 23 m s^{-1}, after which only the first regime is present. However, this statement needs further confirmation, as 30-min averages of wind speed >25 m s^{-1} were not measured during this observational period. We also hypothesize that the wind speed at which the flux sign reversal occurs behaves as a linear function of height. A similar dependence of the lateral momentum flux $\overline{v'w'}$ on wind speed and direction has also been observed (not shown).

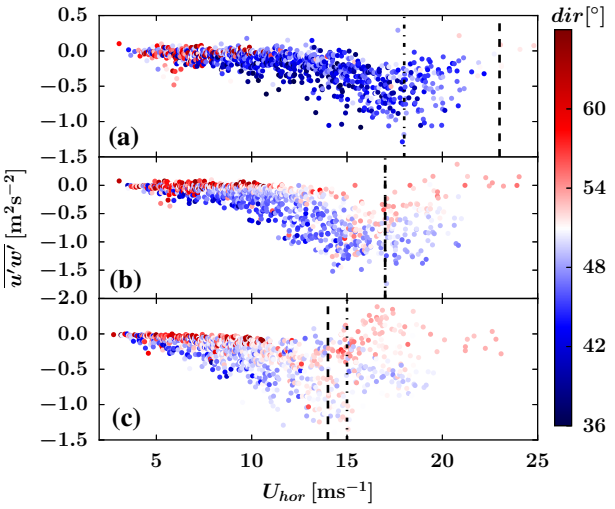

Fig. 8 Scatterplot of 30-min averages of the $\overline{u'w'}$ momentum flux versus the mean horizontal wind speed on **a** 40 m, **b** 22 m and **c** 10 m, for all 17 episodes. *Dots* are colour-coded based on the associated wind direction. *Vertical dashed lines* denote the momentum flux reversal wind speeds equal to 23, 17 and 14 m s^{-1}, respectively. *Vertical dash-dotted lines* denote the momentum flux maxima wind speeds equal to 18, 17 and 15 m s^{-1}, respectively

This highly localized and narrow 15° directional sector, from which the highest wind speeds and the two different momentum flux regimes originate, suggests an important role of the upwind heterogeneities in the complex terrain of Pometeno Brdo. As such, these heterogeneities may have an effect on the high speed coherent structures encountering the hill.

3.5 Analysis of Bora Coherent Structures

To better understand how the topology of coherent structures during bora might be related to the observed momentum flux behaviour, we apply the VITA method to the entire 5-day bora event. Being one of the more robust structure detection techniques, the VITA technique has often been applied for detecting coherent structure occurences. Ever since its introduction in fluid mechanics for purposes of studying the wall structure of low Reynolds number R_e turbulent water-channel flows (Blackwelder and Kaplan 1976; Johansson and Alfredsson 1982), the technique has been extended to high R_e, ABL specific flows. Kailas and Narasimha (1994) have applied the method to near-neutral measurements of the streamwise velocity component u at Boulder, Colorado and Cabauw, Netherlands. In their study of plume transport efficiency in a marine ABL, Mason et al. (2002) have applied VITA to the detection of thermal updrafts and downdrafts by choosing the raw $u'w'$ time series as their detecting variable. Segalini and Alfredsson (2012) have applied both wavelet covariance analysis and the VITA method to detect coherent structures above a forest canopy, and have found qualitatively similar results using both methods.

Using the intermittent nature of the localized, short-time variations in the time series of a detecting variable s, the VITA variance can be defined as (Kailas and Narasimha 1994),

$$D(t; T_{\mathrm{av}}, s) = \frac{1}{T_{\mathrm{av}}} \int_{t-T_{\mathrm{av}}/2}^{t+T_{\mathrm{av}}/2} s'^2(t)\,\mathrm{d}t - \left[\frac{1}{T_{\mathrm{av}}} \int_{t-T_{\mathrm{av}}/2}^{t+T_{\mathrm{av}}/2} s'(t)\,\mathrm{d}t\right]^2, \tag{4}$$

where T_{av} is the averaging time. By using a threshold level k, it is possible to detect the occurence of an event according to,

$$D(t; T_{\mathrm{av}}, s) \geq k\hat{p}^2, \tag{5a}$$

$$\hat{p}^2 = \lim_{T_{\mathrm{av}} \to \infty} D(t; T_{\mathrm{av}}, s), \tag{5b}$$

where $\hat{p}^2$ is the long-term variance of the time series s. The event occurence is defined as the midpoint of the event interval. Finally, after the occurences of all events have been determined, a conditional average of all events is calculated according to,

$$\langle s(\tau) \rangle = \frac{1}{N} \sum_{n=1}^{N} s(t_n + \tau), \tag{6}$$

where τ is the time relative to the occurence, N is the total number of events and t_n is the occurence itself. The flexibility of VITA lies in selecting the values of the key parameters k and T_{av}. Low values of k ensure stronger statistical accuracy, while larger k values capture only the strongest events. The averaging time T_{av} should ideally be on the order of magnitude of the events being observed.

Since the longitudinal wind-speed component perturbations u' have most often been used as the detecting variable in VITA applications, we use the same approach. To determine the best combination of k and T_{av} for proper coherent structure detection, inspection of the occurence frequency as a proxy for the most representative structure embedded in the flow field (Segalini and Alfredsson 2012) has revealed that $k = 1$ and $T_{\mathrm{av}} = 4$ s represents the most effective detection criterion (not shown). To obtain an appreciation of the topology of the coherent structure in terms of all three wind-speed perturbations (Segalini and Alfredsson 2012), the event occurence (based on u' alone) has been extended to both v' and w' for each height separately. Additionally, distinction has been made between structures that represent an acceleration ($\mathrm{d}u'/\mathrm{d}t > 0$) and a retardation ($\mathrm{d}u'/\mathrm{d}t < 0$) during the passage of the structure. Results are presented in Fig. 9.

Granted that some of the VITA uncertainty may lie in the combination of k and T_{av} being slightly dependent on wind speed, stability or some other factor, Fig. 9 shows relatively good event occurence (again, based on u' alone). Noise that is present in the shapes of the lateral and vertical velocity perturbations might also be attributed to the relatively short length of the bora event used to calculate the conditional averages in Eq. 6 (123 h versus, for example, 750 h analyzed by Segalini and Alfredsson (2012). If conditional averages of u' and w' are analyzed in combination, four distinctly different motions are possible, depending on the sign of each of the two fluctuating components of which the flux is composed: outward interaction ($c' > 0,\ w' > 0$), ejection ($c' < 0,\ w' > 0$), inward interaction ($c' < 0,\ w' < 0$), and sweep ($c' > 0,\ w' < 0$), where c is either u or v. It is apparent that an acceleration represents an ejection-sweep cycle, while retardations represent sweep-ejection cycles. In terms of the u' ramp intensity (defined as the amplitude across the event), both cycles are approximately equal, even across all three levels. However, when considering only the vertical velocity structure w' for both cycles, an increase of w' at the 22-m level is obvious. Furthermore, this increase occurs only during the sweep part of the cycle, and is more pronounced during retardations. Hence, it would seem that sweep motions may be responsible for the unusual momentum flux behaviour analyzed thus far. At 10- and 40-m levels, the ejection part of the cycle would be the dominant contributor to the overall momentum flux. Interestingly, for the case of accelerations, at these two levels very weak outward interactions occur.

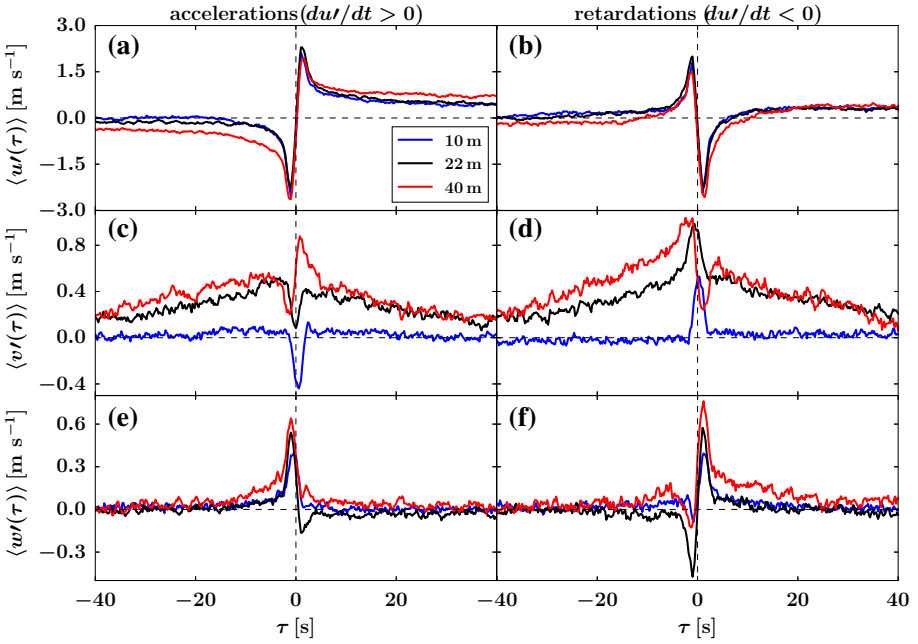

Fig. 9 Accelerating (**a**, **c**, **e**) and retarding (**b**, **d**, **f**) coherent structures detected using the VITA method, based on the entire 123-h bora event, plotted as function of the lag time τ (relative to the event detection $\tau = 0$). Conditional averages are computed for all three wind speed components, based on the event detection in u'. *Dashed vertical and horizontal lines* denote the event occurence and zero perturbation in the wind field, respectively

On the other hand, the v' structure shows a similar topology found by Segalini and Alfredsson (2012), i.e. a sharp jump (of the opposite sign for accelerations and retardations, respectively) around the event occurence. In both cases, the conditionally-averaged v' at the 10- and 22-m levels seem to be in phase, however this is not the case with the 40-m level. Looking back at the time series of the $\overline{v'w'}$ momentum flux shown earlier (Fig. 4c), we hypothesize that this phase displacement might be a possible cause of the negative correlation observed between $\overline{v'w'}$ at the 10- and 40-m levels (especially evident on 24 February).

4 Discussion

Based on the results presented, it is evident that the momentum flux behaviour at the 22-m level and the associated momentum flux divergence show an extreme sensitivity to wind speed and wind direction, and a moderate sensitivity to stratification. In terms of coherent structures impinging on Pometeno Brdo, further insight into the nature of this behaviour was obtained. However, due to the rather complex nature of Pometeno Brdo, it should be emphasized that the degree to which this complexity might interact with the flow in general should be determined. That is, the influence of terrain versus the general flow over Pometeno Brdo on the flux divergence should be disentangled.

Firstly, unusually high values of the lateral momentum flux $\overline{v'w'}$ require explanation. In a rotated coordinate system, this flux is expected to be negligible, compared to the streamwise momentum flux $\overline{u'w'}$. This issue becomes important when considering another requirement

for the validity of MOST. Specifically, this requirement states that the relative off-wind angle, defined as,

$$\alpha = \arctan\left(-\overline{v'w'}/-\overline{u'w'}\right), \tag{7}$$

should be approximately equal to zero if the total horizontal stress vector and the mean wind vector are parallel. Kral et al. (2014), in their observational study of fluxes over a fjord, have found significant values of α depending on the upwind fetch. Over different areas of the Bolund Hill, Berg et al. (2011) have also found significant values of $\overline{v'w'}$, emphasizing the potential importance of the Coriolis force. Additionally, both baroclinicity and non-stationarity may increase the magnitude of α.

Secondly, to determine if the observed momentum flux divergence is strictly tied to bora, wind-direction sectors other than the north-east should be considered. For this purpose, three scirocco events (next to bora, climatologically another important flow at the Adriatic Coast), as well as a 4-day uninterrupted thermally-driven event, have been analyzed in a manner similar to the above (not shown). Namely, time series of momentum fluxes have been analyzed. Surprisingly, similar momentum flux divergences (especially for $\overline{v'w'}$) have been observed during the scirocco events, for wind speeds $\geq 10\,\mathrm{m\,s^{-1}}$. However, the sign of this flux was mostly positive (unlike bora, where it was found to be mostly negative). During the thermally-driven event, no significant flux divergence was found, although wind speeds rarely exceeded $5\,\mathrm{m\,s^{-1}}$. This suggests that the observed flux divergence should perhaps be considered as a function of wind speed and the orography in general, and should not be tied to a specific flow over this area (e.g. bora or scirocco). Unfortunately, due to sparse measurements and the wind climatology of this region, the analyses to date have only been performed for bora.

To further facilitate the importance of changes that bora flow may undergo over Pometeno Brdo, it is important to have in mind the extremely complex nature of the Dinaric Alps to the north-east of Pometeno Brdo. Approximately 30 km to the north-east (upwind) of the measurement tower, the bulk of bora in this region of the Adriatic Coast is generated by a 1800 m high mountain range known as Dinara. Between Dinara and Pometeno Brdo, two additional hills (with heights similar to those of Pometeno Brdo), are located. Due to a lack of both observational and numerical studies, it is unknown to what extent these terrain heterogeneities influence rotors, hydraulic jumps and lee waves generated by Dinara. For example, Grubišić and Stiperski (2009), in their analysis of lee-wave resonances over bell-shaped obstacles, have found that valleys between obstacles may significantly modulate the overall lee-wave flow field. In our case, where these separations between obstacles are extremely short, it is unknown to what extent potential modulations may affect the bora flow until the flow finally reaches Pometeno Brdo. Consequently, this may have an impact on the ABL structure over Pometeno Brdo.

Cases of flow impinging onto a perpendicular barrier, similar to our study, have been previously reported (e.g. Cava et al. 2005). By conducting spectral analyses of topographically-forced structures, Cava et al. (2005) emphasized the intermittent nature of contributions to the transport of momentum in the low frequency range, induced by the topography. On the other hand, Helgason and Pomeroy (2012) relate these low-frequency contributions to the gustiness of the flow. Horiguchi et al. (2012) also report the active role of intermittency in the spatio-temporal evolution of these large-scale, coherent structures. Additionally, Dupont et al. (2008) and Horiguchi et al. (2012) also observed an elevated maximum in the momentum flux (their Figs. 7 and 8, respectively), similar to that found at Pometeno Brdo.

5 Conclusion

Data collected during the winter of 2011 at the central eastern Adriatic Coast, at the top of Pometeno Brdo in the lee of the Dinaric Alps, were used to observe vertical profiles of the kinematic vertical fluxes of momentum and heat during typical bora flow. During this period, a total of 17 bora episodes were extracted and analyzed. The bulk of the analysis focused on the evolution of these fluxes during weak to strong bora wind events.

To obtain reliable flux estimates, an appropriate turbulence averaging time scale is required. Weighted power spectral densities, along with the ogive technique, revealed that a 15-min period serves as a suitable averaging time scale. Analyzing vertical fluxes of momentum and heat revealed that the constant-flux layer, usually indicative of an atmospheric surface-layer, is rarely present during bora. This fact is supported by significant momentum flux and heat flux divergences. A larger momentum flux was present at the 22-m level than at the 10- and 40-m levels, but only for bora wind speeds $>12\,\mathrm{m\,s^{-1}}$ and mainly observed during statically weakly stable to nearly neutral conditions. There is a degree of inherent uncertainty present in these stability boundaries, due to the issue of self-correlation. For wind speeds $>12\,\mathrm{m\,s^{-1}}$ spectral analysis revealed that the turbulent intensities of the vertical wind speed for the 22-m level were larger than for the other two levels. Interestingly, two different regimes of the vertical profiles of momentum flux were observed during strong bora for a narrow range of wind directions. For wind directions between 52° and 60°, vertical momentum transport was very weak or even slightly positive while for wind directions between 45° and 52°, slightly stronger downward transport of momentum persisted, but not during strongest bora wind speeds. With an increase in height, the largest observed values of the momentum fluxes shifted towards greater wind speeds in a linear fashion. An unexpected change in the sign of the momentum flux occured at wind speeds of 23, 17 and $14\,\mathrm{m\,s^{-1}}$ at the 40-, 22- and 10-m levels, respectively. This behaviour resulted in almost non-existent vertical transport of momentum for the largest observed wind speeds. Conditional sampling of the coherent structures using the VITA method showed that the sweep part of the sweep-ejection cycle could potentially be a cause of the observed momentum flux divergence. Overall, the observed degree of flux divergence and, consequently, the absence of a constant-flux layer, questions the applicability of MOST for complex terrain sites such as Pometeno Brdo.

The results presented here provide a unique and informative glance at the microscale characteristics of the bora wind at a complex terrain site, with a relatively dense vertical array of high frequency measurements. As this study is currently unique in this sense, we hope it will serve as a motivation for further investigation of bora's turbulent and coherent structure properties, especially in areas along the Adriatic Coast.

Acknowledgments Two anonymous reviewers are acknowledged for their valuable comments that led to a significant improvement of the manuscript. This study was funded by the Croatian Science Foundation project CATURBO, No. 09/151 , and the Croatian Ministry of Science, Education and Sports project BORA, No. 119-1193086-1311. Tower measurement campaign at Pometeno Brdo was organized within the UKF grant 16/8A WINDEX (www.windex.hr), in collaboration with BORA grant. This work was also partially supported by the EU grant WILL4WIND (www.will4wind.hr), contract no. IPA2007-HR-16IPO-001-040507. This work was also partially supported by Office of Naval Research award N00014-11-1-0709 and by NSF Grant ATM-1151445. We thank Sandip Pal for useful discussions. Temple R. Lee is acknowledged for proofreading the manuscript.

References

Babić K, Bencetić Klaić Z, Večenaj Ž (2012) Determining a turbulence averaging time scale by Fourier analysis for the nocturnal boundary layer. Geofizika 29(1):35–51

Bajić A (1989) Severe bora on the northern Adriatic. Part I: Statistical analysis. Raspr-Pap 24:1–9

Bajić A (1991) Application of the two-layer hydraulic theory on the severe northern Adriatic bora. Meteor Rundschau 44:129–133

Barthlott C, Drobinski P, Fesquet C, Dubos T, Pietras C (2007) Long-term study of coherent structures in the atmospheric surface layer. Boundary-Layer Meteorol 125(1):1–24

Bechmann A, Sørensen NN, Berg J, Mann J, Réthoré PE (2011) The Bolund experiment. Part II: Blind comparison of microscale flow models. Boundary-Layer Meteorol 141(2):245–271

Belušić D, Bencetić Klaić Z (2006) Mesoscale dynamics, structure and predictability of a severe Adriatic bora case. Meteorol Z 15(2):157–168

Belušić D, Mahrt L (2012) Is geometry more universal than physics in atmospheric boundary layer flow? J Geophys Res Atmos (1984–2012) 117:D09115

Belušić D, Pasarić M, Orlić M (2004) Quasi-periodic Bora gusts related to the structure of the troposphere. Q J R Meteorol Soc 130(598):1103–1121

Belušić D, Žagar M, Grisogono B (2007) Numerical simulation of pulsations in the bora wind. Q J R Meteorol Soc 133(627):1371–1388

Belušić D, Hrastinski M, Večenaj Ž, Grisogono B (2013) Wind regimes associated with a mountain gap at the northeastern Adriatic coast. J Appl Meteorol Clim 52(9):2089–2105

Bencetić Klaić Z, Belušić D, Grubišić V, Gabela L, Ćoso L (2003) Mesoscale airflow structure over the northern Croatian coast during MAP IOP-a major bora event. Geofizika 20(1):23–61

Berg J, Mann J, Bechmann A, Courtney M, Jørgensen HE (2011) The Bolund Experiment, Part I: Flow over a steep, three-dimensional hill. Boundary-Layer Meteorol 141(2):219–243

Blackwelder R, Kaplan R (1976) On the wall structure of the turbulent boundary layer. J Fluid Mech 76(01):89–112

Bougeault P, Binder P, Buzzi A, Dirks R, Kuettner J, Houze R, Smith R, Steinacker R, Volkert H (2001) The MAP special observing period. Bull Am Meteorol Soc 82(3):433–462

Cava D, Schipa S, Giostra U (2005) Investigation of low-frequency perturbations induced by a steep obstacle. Boundary-Layer Meteorol 115(1):27–45

Diebold M, Higgins C, Fang J, Bechmann A, Parlange MB (2013) Flow over hills: a large-eddy simulation of the bolund case. Boundary-Layer Meteorol 148(1):177–194

Dupont S, Brunet Y, Finnigan J (2008) Large-eddy simulation of turbulent flow over a forested hill: validation and coherent structure identification. Q J R Meteorol Soc 134(636):1911–1929

Enger L, Grisogono B (1998) The response of bora-type flow to sea surface temperature. Q J R Meteorol Soc 124(548):1227–1244

Feigenwinter C, Vogt R (2005) Detection and analysis of coherent structures in urban turbulence. Theor Appl Climatol 81(3–4):219–230

Foken T, Wimmer F, Mauder M, Thomas C, Liebethal C (2006) Some aspects of the energy balance closure problem. Atmos Chem Phys 6(12):4395–4402

Fortuniak K, Pawlak W, Siedlecki M (2013) Integral turbulence statistics over a central European city centre. Boundary-Layer Meteorol 146(2):257–276

Gohm A, Mayr G (2005) Numerical and observational case-study of a deep Adriatic bora. Q J R Meteorol Soc 131(608):1363–1392

Grachev AA, Fairall CW, Persson POG, Andreas EL, Guest PS (2005) Stable boundary-layer scaling regimes: the SHEBA data. Boundary-Layer Meteorol 116(2):201–235

Grant ER, Ross AN, Gardiner BA, Mobbs SD (2015) Field observations of canopy flows over complex terrain. Boundary-Layer Meteorol 156(2):231–251

Grinsted A, Moore JC, Jevrejeva S (2004) Application of the cross wavelet transform and wavelet coherence to geophysical time series. Nonlinear Process Geophys 11(5/6):561–566

Grisogono B, Belušić D (2009) A review of recent advances in understanding the meso-and microscale properties of the severe bora wind. Tellus A 61(1):1–16

Grubišić V (2004) Bora-driven potential vorticity banners over the Adriatic. Q J R Meteorol Soc 130(602):2571–2603

Grubišić V, Stiperski I (2009) Lee-wave resonances over double bell-shaped obstacles. J Atmos Sci 66(5):1205–1228

Helgason W, Pomeroy JW (2012) Characteristics of the near-surface boundary layer within a mountain valley during winter. J Appl Meteorol Clim 51(3):583–597

Högström U (1996) Review of some basic characteristics of the atmospheric surface layer. Boundary-Layer Meteorol 78:215–246
Horiguchi M, Hayashi T, Adachi A, Onogi S (2012) Large-scale turbulence structures and their contributions to the momentum flux and turbulence in the near-neutral atmospheric boundary layer observed from a 213-m tall meteorological tower. Boundary-Layer Meteorol 144(2):179–198
Horvath K, Bajić A, Ivatek-Šahdan S (2011) Dynamical downscaling of wind speed in complex terrain prone to bora-type flows. J Appl Meteorol Soc 50(8):1676–1691
Horvath K, Lin YL, Ivančan-Picek B (2008) Classification of cyclone tracks over the Apennines and the Adriatic Sea. Mon Weather Rev 136(6):2210–2227
Horvath K, Fita L, Romero R, Ivančan-Picek B (2006) A numerical study of the first phase of a deep Mediterranean cyclone: Cyclogenesis in the lee of the Atlas Mountains. Meteorol Z 15(2):133–146
Horvath K, Ivatek-Šahdan S, Ivančan-Picek B, Grubišić V (2009) Evolution and structure of two severe cyclonic bora events: contrast between the northern and southern Adriatic. Weather Forecast 24(4):946–964
Horvath K, Koracin D, Vellore R, Jiang J, Belu R (2012) Sub-kilometer dynamical downscaling of near-surface winds in complex terrain using WRF and MM5 mesoscale models. J Geophys Res-Atmos (1984–2012) 117(D11). doi:10.1029/2011JD016447
Huang NE, Shen Z, Long SR, Wu MC, Shih HH, Zheng Q, Yen NC, Tung CC, Liu HH (1998) The empirical mode decomposition and the Hilbert spectrum for nonlinear and non-stationary time series analysis. Proc R Soc Lond A 454(1971):903–995
Jeromel M, Vlado Malačič V, Rakovec J (2009) Weibull distribution of bora and sirocco winds in the northern Adriatic Sea. Geofizika 26(1):85–100
Johansson AV, Alfredsson PH (1982) On the structure of turbulent channel flow. J Fluid Mech 122:295–314
Jurčec V (1981) On mesoscale characteristics of bora conditions in Yugoslavia. Weather and weather maps. Springer, New York, pp 640–657
Kailas SV, Narasimha R (1994) Similarity in VITA-detected events in a nearly neutral atmospheric boundary layer. Proc R Soc Lond 447(1930):211–222
Kaimal JC, Finnigan JJ (1994) Atmospheric boundary layer flows: their structure and measurement. Oxford University Press, Oxford 304 pp
Klemp J, Durran D (1987) Numerical modelling of bora winds. Meteorol Atmos Phys 36(1–4):215–227
Kral ST, Sjöblom A, Nygård T (2014) Observations of summer turbulent surface fluxes in a High Arctic fjord. Q J R Meteorol Soc 140(679):666–675
Krusche N, De Oliveira AP (2004) Characterization of coherent structures in the atmospheric surface layer. Boundary-Layer Meteorol 110(2):191–211
Kuettner J, O'Neill T (1981) ALPEX-the GARP mountain subprogram. Bull Am Meteorol Soc 62(6):793–805
Lee X, Massman W, Law BE (2004) Handbook of micrometeorology: a guide for surface flux measurement and analysis. Kluwer Academic Publishers, Dordrecht 250 pp
Lepri P, Kozmar H, Večenaj Ž, Grisogono B (2014) A summertime near-ground velocity profile of the Bora wind. Wind Struct 19(5):505–522
Lopes AS, Palma J, Castro F (2007) Simulation of the Askervein flow. Part 2: large-eddy simulations. Boundary-Layer Meteorol 125(1):85–108
Lundquist JK (2003) Intermittent and elliptical inertial oscillations in the atmospheric boundary layer. J Atmos Sci 60(21):2661–2673
Mahrt L (2007) The influence of nonstationarity on the turbulent flux-gradient relationship for stable stratification. Boundary-Layer Meteorol 125:245–264
Mahrt L, Gamage N (1987) Observations of turbulence in stratified flow. J Atmos Sci 44:1106–1121
Mason RA, Shirer HN, Wells R, Young GS (2002) Vertical transports by plumes within the moderately convective marine atmospheric surface layer. J Atmos Sci 59(8):1337–1355
Metzger M, Holmes H (2008) Time scales in the unstable atmospheric surface layer. Boundary-Layer Meteorol 126(1):29–50
Moncrieff J, Clement R, Finnigan J, Meyers T (2004) Averaging, detrending, and filtering of eddy covariance time series. Handbook of micrometeorology. Springer, New York, pp 7–31
Monin A, Obukhov A (1954) Basic laws of turbulent mixing in the surface layer of the atmosphere. Contrib Geophys Inst Acad Sci USSR 151:163–187
Moreira GA, Dos Santos AA, Do Nascimento CA, Valle RM (2012) Numerical study of the neutral atmospheric boundary layer over complex terrain. Boundary-Layer Meteorol 143(2):393–407
Nadeau DF, Pardyjak ER, Higgins CW, Parlange MB (2013) Similarity scaling over a steep alpine slope. Boundary-Layer Meteorol 147(3):401–419
Oncley SP, Friehe CA, Larue JC, Businger JA, Itsweire EC, Chang SS (1996) Surface-layer fluxes, profiles, and turbulence measurements over uniform terrain under near-neutral conditions. J Atmos Sci 53(7):1029–1044

Petkovšek Z (1976) Periodicity of bora gusts. Razpr–Pap SMD 20:67–75
Petkovšek Z (1982) Gravity waves and bora gusts. Ann Meteorol (NF) 19:108–110
Petkovšek Z (1987) Main bora gusts—a model explanation. Geofizika 4:41–50
Poje D (1992) Wind persistence in Croatia. Int J Climatol 12(6):569–586
Reynolds O (1894) On the dynamical theory of incompressible viscous fluids and the determination of the criterion. Proc R Soc Lond 56(336–339):40–45
Robinson SK (1991) Coherent motions in the turbulent boundary layer. Annu Rev Fluid Mech 23(1):601–639
Segalini A, Alfredsson PH (2012) Techniques for the eduction of coherent structures from flow measurements in the atmospheric boundary layer. Boundary-Layer Meteorol 143(3):433–450
Smith RB (1987) Aerial observations of the Yugoslavian bora. J Atmos Sci 44(2):269–297
Stull RB (1988) An introduction to boundary layer meteorology. Kluwer Academic Publishers, Dordrecht 666 pp
Thomas C, Foken T (2007) Flux contribution of coherent structures and its implications for the exchange of energy and matter in a tall spruce canopy. Boundary-Layer Meteorol 123(2):317–337
Torrence C, Compo GP (1998) A practical guide to wavelet analysis. Bull Am Meteorol Soc 79(1):61–78
Undheim O, Andersson H, Berge E (2006) Non-linear, microscale modelling of the flow over Askervein Hill. Boundary-Layer Meteorol 120(3):477–495
Van der Hoven I (1957) Power spectrum of horizontal wind speed in the frequency range from 0.0007 to 900 cycles per hour. J Meteorol 14(2):160–164
Večenaj Ž, Belušić D, Grisogono B (2010) Characteristics of the near-surface turbulence during a bora event. Ann Geophys 28:155–163
Večenaj Ž, De Wekker SFJ (2014) Determination of non-stationarity in the surface layer during the T-REX experiment. Q J R Meteorol Soc 141(690):1560–1571
Večenaj Ž, De Wekker SFJ, Grubišić V (2011) Near-surface characteristics of the turbulence structure during a mountain-wave event. J Appl Meteorol Clim 50(5):1088–1106
Večenaj Ž, Belušić D, Grubišić V, Grisogono B (2012) Along-coast features of bora-related turbulence. Boundary-Layer Meteorol 143(3):527–545
Vickers D, Mahrt L (1997) Quality control and flux sampling problems for tower and aircraft data. J Atmos Ocean Tech 14(3):512–526
Vickers D, Mahrt L (2006) A solution for flux contamination by mesoscale motions with very weak turbulence. Boundary-Layer Meteorol 118(3):431–447
Whiteman CD (2000) Mountain meteorology: fundamentals and applications. Oxford University Press, Oxford 355 pp
Wilczak JM, Oncley SP, Stage SA (2001) Sonic anemometer tilt correction algorithms. Boundary-Layer Meteorol 99(1):127–150
Yoshino M (1976) Local wind bora: a research summary. University of Tokyo Press, Tokyo, pp 277–282
Zeri M, Sá LDdA (2011) Scale dependence of coherent structures' contribution to the daytime buoyancy heat flux over the Pantanal wetland, Brazil. Atmos Sci Lett 12(2):200–206